

# Metallicity dependence of the s–process in massive stars: theoretical predictions

M. Pignatari and R. Gallino

Dipartimento di Fisica Generale, Università di Torino, Via P. Giuria 1, 10125 Torino, Italy  
e-mail: mpignatari@gmail.com

**Abstract.** At solar–like metallicity the s–process (slow neutron capture process) in massive stars ( $M \geq 10M_{\odot}$ ) is efficient during convective core He–burning and convective shell C–burning. In both the two phases the  $^{22}\text{Ne}(\alpha, n)^{25}\text{Mg}$  reaction is the main neutron source. However, moving to metallicities lower than solar, the C shell contribution to the total neutron exposure  $\tau$  becomes marginal with respect to the s–process contribution in the He core. For this reason, at low metallicity the s–process signature beyond iron is mainly given by the He core. In these conditions, the definition of the  $^{22}\text{Ne}$  abundance in the last phases of the He core is crucial for the weak s–process behaviour. Without considering nuclear and models development uncertainties, the initial isotopic distribution of light isotopes severely affects the final s–process distribution. In particular, this point is related to the spectroscopic observations discrepancy of oxygen, that is the most abundant element within the initial CNO nuclei which are converted in the main neutron source  $^{22}\text{Ne}$ .

## 1. Introduction

The weak s–process in massive stars produces most of the s–isotopes between the iron peak and the strontium peak ( $26 \leq Z \leq 38$ ) present in the solar system (Raiteri et al. 1993) (weak s–process component). A minor contribution is due to the main s–process component from AGB stars, which generally increases with increasing  $Z$  (Arlandini et al. 1999).

At solar metallicity the main contribution to the final s–process yields is given by convective core He–burning and convective shell C–burning (Raiteri et al. 1993; Pignatari et al. 2006; The, El Eid, & Meyer 2007). The  $^{22}\text{Ne}(\alpha, n)^{25}\text{Mg}$  reaction is the main neutron source in both the two phases. The major part of neutrons are captured by light isotopes be-

cause of their high abundance. However,  $^{56}\text{Fe}$  captures an important amount of neutrons feeding the heavier isotopes. In these conditions, the s–process efficiency falls beyond the Sr peak because of the low neutron exposure  $\tau$ .

The most important light neutron poison (i.e. neutron absorber) at solar metallicity is  $^{25}\text{Mg}$ . However, the most efficient neutron absorber should be the  $^{16}\text{O}$  produced in the He core as primary (i.e. it is produced starting from initial H and He and does not depend on the initial metallicity of the star) and is the most abundant isotope at the end of the He core. However, neutrons captured by  $^{16}\text{O}$  are re–emitted via the  $^{17}\text{O}(\alpha, n)^{20}\text{Ne}$  reaction (neutron recycling effect). The  $^{16}\text{O}$  produced in the He core has not to be confused with the initial one that is all converted in  $^{14}\text{N}$  by the CNO cycle in the previous H–burning core.

---

Send offprint requests to: M. Pignatari

The main neutron source  $^{22}\text{Ne}$  is secondary, i.e. its abundance depends on the initial metallicity of the star. We said that almost all the CNO nuclei are converted in  $^{14}\text{N}$  via the CNO cycle in H-burning conditions. Then, via the  $\alpha$ -capture channel  $^{14}\text{N}(\alpha,\gamma)^{18}\text{F}(\beta^+)^{18}\text{O}(\alpha,\gamma)^{22}\text{Ne}$   $^{14}\text{N}$  is totally converted in  $^{22}\text{Ne}$  when in core He-burning the temperature is higher than  $2.5 \cdot 10^8$  K. For this reason, the amount of the neutron source  $^{22}\text{Ne}$  is defined by the initial CNO nuclei. Within CNO, oxygen is the most abundant element (and  $^{16}\text{O}$  is 99.76 % of the oxygen in the solar system). Moving to low metallicity calculations, for light elements an initial solar scaled composition is a wide approximation. Different spectroscopic observations of stars with different metallicity define two possible scenarios for the oxygen trend with respect to metallicity:

- first scenario -  $[\text{O}/\text{Fe}]$  ( $\text{O}/\text{Fe}$  within square brackets means that  $\text{O}/\text{Fe}$  ratio is normalized to the solar ratio) linearly increases going from  $[\text{Fe}/\text{H}] = 0$  to  $[\text{Fe}/\text{H}] = -1$  (disk stars). In the halo stars ( $[\text{Fe}/\text{H}] < -1$ ),  $[\text{O}/\text{Fe}]$  shows a flat enhancement by 0.3–0.5 dex (Gratton & Ortolani 1986; Ryan et al. 1991);
- second scenario -  $[\text{O}/\text{Fe}]$  linearly increases going from  $[\text{Fe}/\text{H}] = 0$  to lower metallicity, also for  $[\text{Fe}/\text{H}] < -1$  (Abia & Rebolo 1989; Mishenina et al. 2000; Israelian et al. 2001). For example, (Mishenina et al. 2000)  $[\text{O}/\text{Fe}] = -0.37[\text{Fe}/\text{H}] + 0.047$ .

In stellar spectroscopic analysis oxygen may be observed using the O I triplet at 7774 Å, the [OI] forbidden line at 6300 Å, the molecular OH lines in the UV band. O I triplet observation seems to be affected by deviation from LTE assumption going to low metallicity, producing a higher  $[\text{O}/\text{Fe}]$  in the observations. However, the effective deviation is still not well known (Kiselman 1991; Takeda 2003). Other systematic errors in the different references could be included by different atmospheric models and/or by different atmospheric parameters. Moreover, (Asplund & García Pérez 2001) showed that using 3D atmospheric models instead of classic 1D models the  $[\text{O}/\text{Fe}]$

measured from OH lines is strongly lower, depending on the atmospheric parameters. In this paper we consider both the two scenarios presented, looking at the consequences in the s-process calculations.

" $\alpha$ -enhancements" for the  $\alpha$ -rich nuclei  $^{20}\text{Ne}$ ,  $^{24}\text{Mg}$ ,  $^{28}\text{Si}$  are included, and those of  $^{32}\text{S}$ ,  $^{36}\text{Ar}$ ,  $^{39}\text{K}$ ,  $^{40}\text{Ca}$  and  $^{48}\text{Ti}$  (Raiteri et al. 1992).  $[\text{X}_i/\text{Fe}]$  linearly increases going from  $[\text{Fe}/\text{H}] = 0$  to  $[\text{Fe}/\text{H}] = -1$  (disk stars). In the halo stars ( $[\text{Fe}/\text{H}] < -1$ ),  $[\text{X}_i/\text{Fe}]$  has a flat enhancement. In Table 1, the enhancements factors extrapolated from (Reddy et al. 2003) and used in our calculations are listed. The other stable isotopes that belong to Ne, Mg, Si, S, K, Ca and Ti are assumed to be solar scaled.

Results for 25  $M_{\odot}$  models (Käppeler et al. 1994) with an updated nuclear network are presented at  $[\text{Fe}/\text{H}] = -1, -2$  compared to the solar metallicity case using both the  $[\text{O}/\text{Fe}]$  vs  $[\text{Fe}/\text{H}]$  profiles. In the first scenario  $^{16}\text{O}$  has an enhancement  $\alpha = +0.5$  for  $[\text{Fe}/\text{H}] < -1$  (models labelled with "A", e.g. M25Z2M3A means a 25  $M_{\odot}$  and  $[\text{Fe}/\text{H}] = -1$  model, with oxygen enhancement A).  $\alpha$ -enhancements listed in Table 1 are included. The other isotopes are assumed to be solar scaled. In the second scenario  $^{16}\text{O}$  is assumed to linearly increase with decreasing the metallicity ( $[\text{O}/\text{Fe}] = -0.4[\text{Fe}/\text{H}]$ , models labelled with "B", e.g. M25Z2M4B means a 25  $M_{\odot}$  and  $[\text{Fe}/\text{H}] = -2$  model, with oxygen enhancement B). The other stable isotopes are assumed to be solar scaled. Similar calculations are presented in (Pignatari et al. 2006) for a 25  $M_{\odot}$  and  $[\text{Fe}/\text{H}] = -1$  model compared to the solar metallicity case with an initial solar scaled composition for all isotopes.

## 2. Calculations

The stellar code FRANEC (version of Chieffi & Straniero 1989) follows the 25  $M_{\odot}$  star evolution up to the end of the He-burning core. During this phase, a post-processing multi-zone code follows the s nucleosynthesis (Käppeler et al. 1994).

A one-zone post-processing model follows the nucleosynthesis in the C shell. With respect to the previous He core model, the C

**Table 1.**  $\alpha$ –enhancements in our set of calculations at  $[\text{Fe}/\text{H}] = -1, -2$  (see the text).

Isotope	$\alpha$ –enhancement $[\text{X}_i/\text{Fe}] = +\alpha$
$^{20}\text{Ne}$	0.27
$^{24}\text{Mg}$	0.27
$^{28}\text{Si}$	0.10
$^{32}\text{S}$	0.10
$^{36}\text{Ar}$	0.10
$^{39}\text{K}$	0.10
$^{40}\text{Ca}$	0.17
$^{48}\text{Ti}$	0.25

shell network is extended and it includes unstable isotopes with terrestrial  $\beta^-$  decay half lives longer than 5 min (see also Pignatari et al. 2006). The reason is that in convective C shell conditions the neutron density reaches  $10^{11}–10^{12}$   $\text{n}\cdot\text{cm}^{-3}$  or higher values in the last days before the supernova explosion. At the C ignition in the C shell initial abundances are assumed to be the abundances obtained at the He exhaustion in the core. The reason is that C shell burns over the ashes of the previous convective He core. However, at metallicity lower than solar in the total neutron exposure the C shell contribution rapidly decreases with respect to the solar metallicity case (Pignatari et al. 2006), and the final s–process distribution is almost fully obtained already at the end of the He core. The reason is that in C–burning conditions the primary neutron poison efficiency is higher with respect to He–burning. Recycling of neutrons captured by  $^{16}\text{O}$  via  $^{17}\text{O}(\alpha, n)^{20}\text{Ne}$  is only partially efficient. Moreover,  $^{20}\text{Ne}$  that in the He core was a secondary neutron poison in the C shell is produced in a primary way by the  $^{12}\text{C}(^{12}\text{C}, \alpha)^{20}\text{Ne}$  reaction and it is a primary neutron poison, like  $^{16}\text{O}$  and  $^{23}\text{Na}$ .

In §2.1,2.2 we present our results obtained at the end of the C shell in the region interested by He core + C shell nucleosynthesis. Such results will be presented in more details in a next paper.

### 2.1. $25 M_{\odot}$ models "A"

Figure 1 shows the weak s distribution between  $^{57}\text{Fe}$  and  $^{93}\text{Nb}$  at the end of the C shell for a  $25$

$M_{\odot}$  and  $[\text{Fe}/\text{H}] = -1, -2$  compared with the solar metallicity case. The initial isotopic abundances set at low metallicity is given in agreement with the scenario "A".

Because of the enhancements, going from  $[\text{Fe}/\text{H}] = 0$  to  $[\text{Fe}/\text{H}] = -1$  several isotopes (we remind that in this case of  $^{16}\text{O}$   $\alpha=+0.5$ ) change their relative abundances. This means that the neutron source  $^{22}\text{Ne}$  versus neutron poisons initial abundances is changed. In the Cu region just beyond Fe the secondary–like trend with the metallicity of the s distribution is confirmed, as it is obtained using an initial solar scaled composition (Pignatari et al. 2006). This means that the s–process behavior in this region is not affected by the uncertainty in oxygen spectroscopic observations.

On the other hand, going to heavier elements up to the Sr peak region the abundances normalized to solar of the  $25 M_{\odot}$  and  $[\text{Fe}/\text{H}] = -1$  model moves to the solar model values, showing in the Sr peak a primary–like behavior within the uncertainties.

Going from  $[\text{Fe}/\text{H}] = -1$  to  $[\text{Fe}/\text{H}] = -2$ , the neutron source versus neutron poisons relation is the same (all the enhancements included now shows a flat behavior with the metallicity), but at  $[\text{Fe}/\text{H}] = -2$  the  $^{16}\text{O}$  neutron poisoning effect becomes more efficient and the process is more than secondary–like.

### 2.2. $25 M_{\odot}$ models "B"

Figure 2 shows the weak s distribution between  $^{57}\text{Fe}$  and  $^{93}\text{Nb}$  at the end of the C shell for  $25 M_{\odot}$  and  $[\text{Fe}/\text{H}] = -1, -2$  models compared with

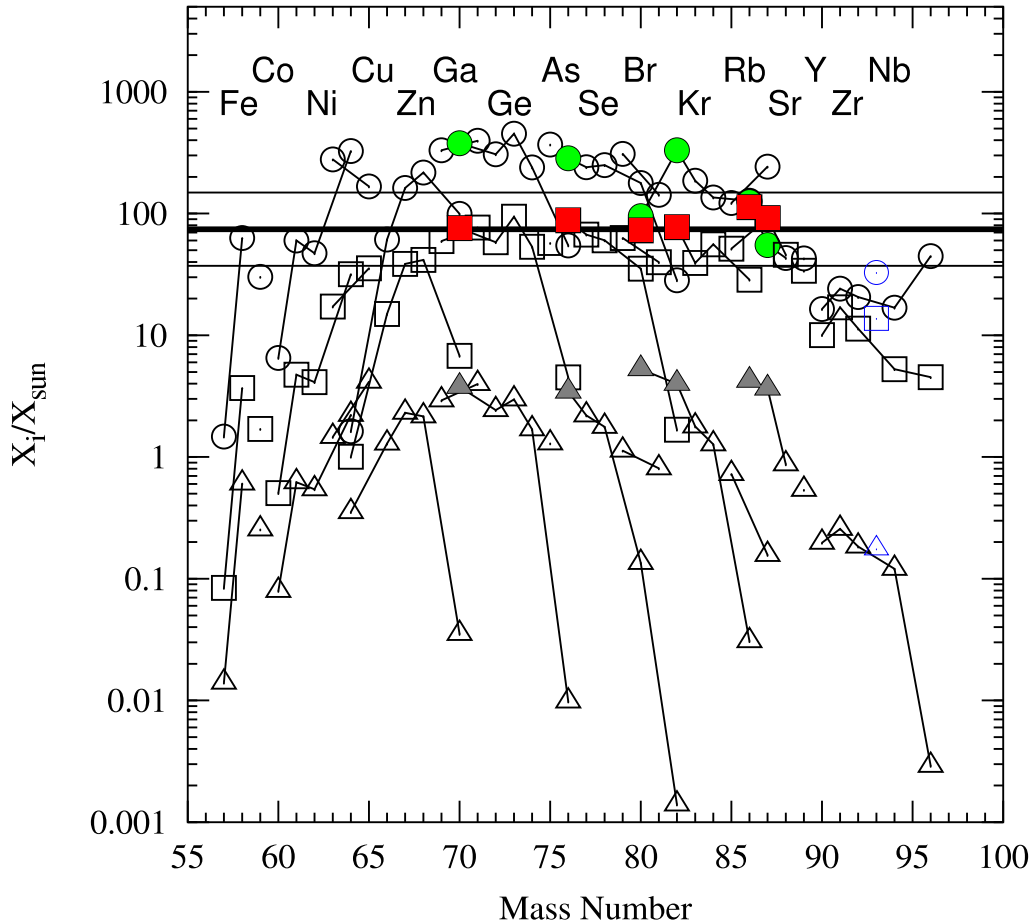


**Fig. 1.** Abundances normalized to solar (Anders & Grevesse 1989) at the end of the C shell for HE25Z2M3A (squares) and HE25Z2M4A (triangles) cases compared with the solar metallicity case (circles). See the text for the label explanation. Full marks are the  $s$ -only isotopes (green circles, red squares and grey triangles respectively), the other stable isotopes are reported in black empty marks, with the exception of  $^{93}\text{Nb}$ , that is reported with a blue empty mark to distinguish it from Zr isotopes.  $^{16}\text{O}$  overabundance is reported at the He exhaustion (thick line), multiplied and divided by a factor of two (thin lines).  $25 M_{\odot}$  and  $[\text{Fe}/\text{H}] = 0, -1, -2$ ; initial composition from the 1st scenario (see the text for explanation).

the solar metallicity case. The initial isotopic abundances set at low metallicity is given in agreement with the scenario "B".

Like in the previous case, going from  $[\text{Fe}/\text{H}] = 0$  to  $[\text{Fe}/\text{H}] = -1$   $\alpha$ -enhanced isotopes (we remind that at  $[\text{Fe}/\text{H}] = -1$   $^{16}\text{O}$   $\alpha=+0.4$  and still increases going to lower metallicity) change their relative abundances. In the Cu region the result obtained in §2.1 is

confirmed, and the primary-like trend going to the Sr peak as well.

However, the primary-like nature of the Sr peak isotopes is confirmed also in the  $25 M_{\odot}$  and  $[\text{Fe}/\text{H}] = -2$  model. The reason is that the  $\alpha$ -enhancement of oxygen at  $[\text{Fe}/\text{H}] = -2$  is  $\alpha=+0.8$  and the  $^{22}\text{Ne}$  abundance with respect to the neutron poisons abundance is high enough to give an efficient  $s$  nucleosynthesis. On the other hand, the secondary-like

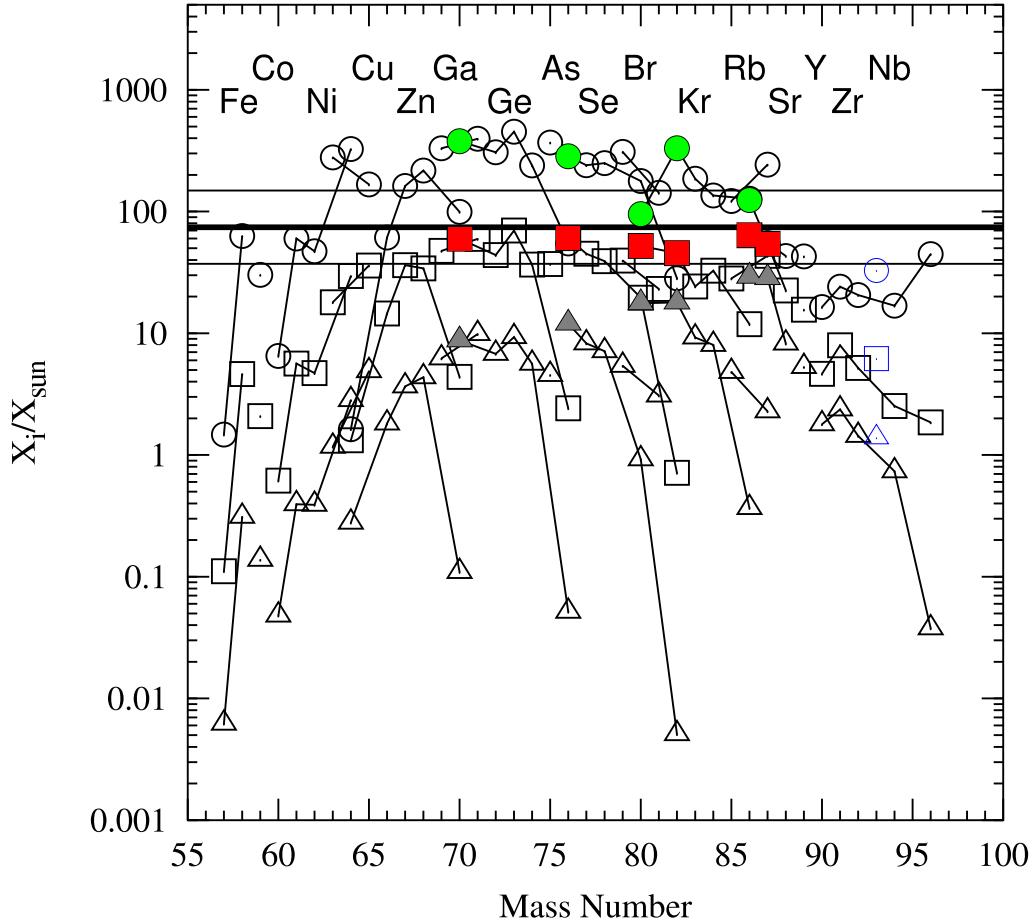


**Fig. 2.** The same plot presented in Figure 1 is reported for the  $25 M_{\odot}$  and  $[\text{Fe}/\text{H}] = -1, -2$  models compared with the solar metallicity model, where the initial isotopic composition is given by the 2nd scenario (see the text for explanation). M25Z2M3B, M25Z2M4B.

Cu trend with the metallicity is confirmed. This result is in agreement with the spectroscopic observations of this element at low metallicity (Bisterzo et al. 2005).

### 3. Conclusions

The  $[\text{O}/\text{Fe}]$  trend with respect to  $[\text{Fe}/\text{H}]$  affects the  $^{22}\text{Ne}$  amount that provides neutrons for the s-process. We present a set of calculations for a  $25 M_{\odot}$  model at different metallicities chang-

ing the  $^{16}\text{O}$  initial abundance within the observations uncertainty.

The weak s component is generally considered secondary-like. However, the s-process calculations show how this assumption is affected by the adopted initial composition set. We concluded that along the s path beyond Fe the Cu region show a secondary-like trend, despite different assumptions for the initial abundance distributions. However, looking at the Kr-Sr region the initial abundance set used in the calculations may affect the metallicity de-

pendence of the s distribution. In particular, using a linear increase of [O/Fe] with decreasing [Fe/H] (scenario "B" in the text) down to [Fe/H] = -2 the Sr peak region shows an almost primary behavior. On the other hand, using a flat behavior of [O/Fe] vs [Fe/H] below [Fe/H] = -1 (scenario "A" in the text) the primary nature of the s distribution in the Sr peak region is conserved down to [Fe/H] = -1 and it becomes almost secondary-like below this metallicity.

### References

- Abia, C., & Rebolo, R. 1989, *ApJ*, 347, 186  
 Anders, E., & Grevesse, N. 1989, *Geoch. Cosmoch. Acta*, 53, 197  
 Arlandini, C., Käppeler, F., Wisshak, K., et al. 1999, *ApJ*, 525, 886  
 Asplund, M. & García Pérez, A. E. 2001, *A&A*, 372, 302  
 Bisterzo, S., et al. 2005, *Nuc. Phys. A*, 758, 284  
 Chieffi, A., & Straniero, O. 1989, *ApJS*, 71, 47  
 Gratton, R. G., & Ortolani, S. 1986, *A&A*, 169, 201  
 Israelian, G., et al. 2001, *ApJ*, 551, 833  
 Kiselman, D. 1991, *A&A*, 245, 9  
 Käppeler, F., et al. 1994, *ApJ*, 437, 396  
 Mishenina, T., V., et al. 2000, *A&A*, 353, 978  
 Pignatari, M., et al. 2006, *PoS*, 061  
 Raiteri, C. M., et al. 1992, *ApJ*, 387, 263  
 Raiteri, C. M., et al. 1993, *ApJ*, 419, 207  
 Reddy, B., E., et al. 2003, *MNRA Soc.*, 340, 304  
 Ryan, S. G., et al. 1991, *AJ*, 102, 303  
 Takeda, Y. 2003, *A&A*, 402, 343  
 The, L.-S., El Eid, M. F., & Meyer, B. S. 2007, *ApJ*, 655, 1058  
 Travaglio, C. 2004, *ApJ*, 601, 864